RESEARCH ARTICLE

NANO · MICRO small
www.small-journal.com

Ultraviolet Circularly Polarized Luminescence in Chiral Perovskite Nanoplatelet-Molecular Hybrids: Direct Binding Versus Efficient Triplet Energy Transfer

Bing Tang, Qi Wei, Shixun Wang, Haochen Liu, Nanli Mou, Qi Liu, Ye Wu, Arsenii S. Portniagin, Stephen V. Kershaw, Xiaoqing Gao, Mingjie Li, and Andrey L. Rogach**

The development of ultraviolet circularly polarized light (UVCPL) sources has the potential to benefit plenty of practical applications but remains a challenge due to limitations in available material systems and a limited understanding of the excited state chirality transfer. Herein, by constructing hybrid structures of the chiral perovskite $CsPbBr_3$ nanoplatelets and organic molecules, excited state chirality transfer is achieved, either via direct binding or triplet energy transfer, leading to efficient UVCPL emission. The underlying photophysical mechanisms of these two scenarios are clarified by comprehensive optical studies. Intriguingly, UVCPL realized via the triple energy transfer, followed by the triplet–triplet annihilation upconversion processes, demonstrates a 50-fold enhanced dissymmetry factor g_{lum}. Furthermore, stereoselective photopolymerization of diacetylene monomer is demonstrated by using such efficient UVCPL. This study provides both novel insights and a practical approach for realizing UVCPL, which can also be extended to other material systems and spectral regions, such as visible and near-infrared.

1. Introduction

The development of circularly polarized light (CPL) sources has received considerable interest due to their potential applications in a wide range of fields, including 3D displays, optical sensors, chiral catalysis, information encryption, and spintronics.[1–8] Conventionally, CPL is mainly realized through the conversion of unpolarized light with the combination of a linear polarizer and quarter-wave plate, which inevitably increases the energy losses, device complexity as well as implementation cost and limits the performance. Therefore, chiral luminescent materials capable of directly generating CPL offer a simple and efficient approach to tackle these challenges and promote their applications in miniaturized devices and highly integrated photonic systems.[2,6,8–12] Consequently, significant research efforts have been dedicated to various CPL-active materials, such as chiral organic molecules, liquid crystals, supramolecular assemblies, and inorganic semiconductor nanocrystals, for achieving emission across a wide spectral range.[3,6,9,13–19] However, limited by the band structures of the realized materials, as well as by a limited understanding of the excited state chirality transfer, most of the reported CPL emission was restricted to the visible range.[6,8–11,13,14] The realization of ultraviolet circularly polarized light (UVCPL) emission with high photon energy would benefit the applications in stereoselective photocatalysis and photopolymerization.[5,20,21] Yet, due to the constraints on the bandgap of the most possible materials, UVCPL was mainly demonstrated using chiral organic compounds,[21,22] whose syntheses require tedious procedures for chirality induction, as well as complex separation and purification techniques. Moreover, an excitation source with even higher photon energy is still necessary for realizing UVCPL emission, which makes their applications rather challenging. On the other hand, recently emerged nanocrystal-molecular hybrids that combine the advantages of inorganic semiconductor quantum dots and organic molecules, provide a promising approach to realize UVCPL.[23–35] According to Kuno et al.,[36] by employing a direct ligand exchange

B. Tang, S. Wang, H. Liu, N. Mou, Q. Liu, Y. Wu, A. S. Portniagin, S. V. Kershaw, A. L. Rogach
Department of Materials Science and Engineering, and Centre for Functional Photonics (CFP)
City University of Hong Kong
83 Tat Chee Avenue, Hong Kong SAR 999077, P. R. China
E-mail: andrey.rogach@cityu.edu.hk
Q. Wei, M. Li
Department of Applied Physics
The Hong Kong Polytechnic University
Hung Hom, Kowloon, Hong Kong SAR 999077, P. R. China
E-mail: ming-jie.li@polyu.edu.hk
X. Gao
Wenzhou Key Laboratory of Biophysics
Wenzhou Institute
University of Chinese Academy of Sciences
Wenzhou 325000, P. R. China

The ORCID identification number(s) for the author(s) of this article can be found under https://doi.org/10.1002/smll.202311639

DOI: 10.1002/smll.202311639

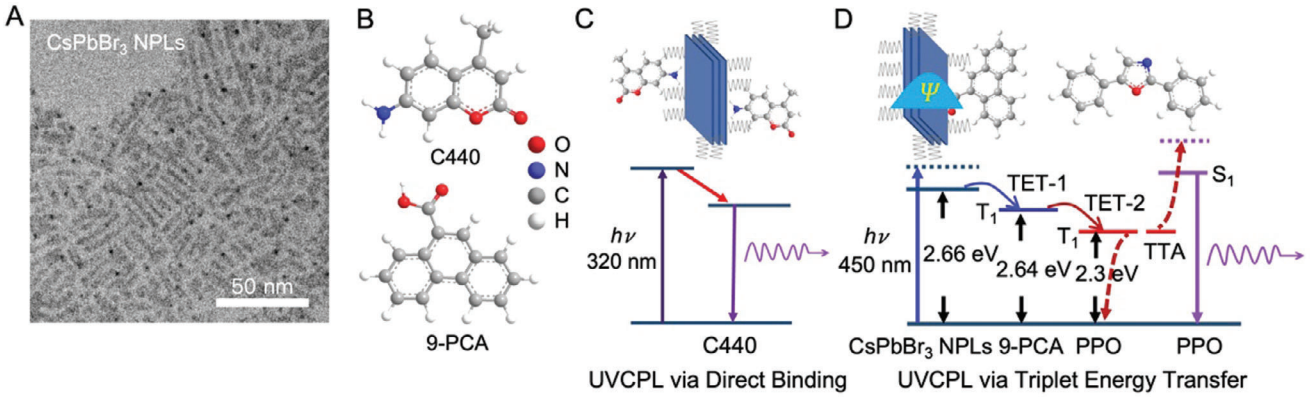

Figure 1. A) TEM image of $CsPbBr_3$ NPLs employed in this study. B) Chemical structures of C440 and 9-PCA molecules. Schemes of nanocrystal-molecular hybrids, shown together with their anticipated energy level schemes and related photophysical processes (which will be discussed later on) comprised of $CsPbBr_3$ NPLs and C440 C) or 9-PCA D) molecules for realizing UVCPL emission via either direct binding or the TET process.

between achiral dyes and chiral inorganic HgS nanocrystals, the former bind at the surface with a chiral motif, and thus realize green CPL emission centered at 525 nm. Moreover, when suitable triplet transmitters are anchored at the surface, UVCPL can be expected from triplet annihilators based on the triplet energy transfer (TET) and a subsequent triplet–triplet annihilation upconversion (TTA-UC) processes.[37–41] However, so far, there have been few reports on the realization of UVCPL in these nanocrystal-molecular hybrids either via direct binding or the TET process. In particular, it's critical to understand whether chiral light harvesting could occur through the TTA-UC process between the chiral inorganic nanocrystals and achiral annihilators.

In this study, we have successfully fabricated perovskite nanocrystal-molecular hybrids consisting of chiral inorganic $CsPbBr_3$ nanoplatelets (NPLs) and achiral organic molecules, resulting in efficient UVCPL emission. Two mechanisms of the excited state chirality transfer occurring either via direct binding or the TET process are revealed and compared. This study provides both novel insights and a practical approach for realizing UVCPL, which can also be extended to other material systems and spectral regions, such as visible and near-infrared.

2. Results and Discussion

Recently, we have reported that $CsPbBr_3$ perovskite NPLs synthesized via an anti-solvent protocol possess intrinsic chirality induced by naturally formed screw dislocations.[42] In this study, because of the optimal bandgap and energy level alignment, $CsPbBr_3$ NPLs comprising 3 monolayers (MLs) were selected as a chiral inorganic counterpart for investigating excited state chirality transfer via either direct binding or the TET process. The bandgap energy of 3 ML $CsPbBr_3$ NPLs is derived as 2.66 eV according to the corresponding Tauc plot in Figure S1 (Supporting Information), blue-shifted as compared to bulk $CsPbBr_3$ (bandgap of 2.4 eV, or 517 nm) due to the quantum confinement effect. As evidenced by transmission electron microscopy (TEM) images shown in Figure S2 (Supporting Information) and **Figure 1**A, these NPLs are chiral twisted ribbons with a thickness of 2.0 ± 0.2 nm, which is much smaller than the Bohr radius of $CsPbBr_3$ (7 nm), meaning that they are indeed in a strong quantum confinement regime. Such chiral perovskite NPLs should be able to provide efficient electronic coupling with organic molecules, leading to efficient chirality transfer via direct binding or the TET process both of which require strong electronic coupling between chiral NPLs and organic molecules.[43–47]

Considering the fluorescence of Coumarin 440 molecules (abbreviated as C440 later on) in toluene and its amine group for binding at NPL's surface (Figure 1B), C440 has been chosen as a potential UVCPL emitter for the direct binding case. UV emission was recorded from C440 dispersed in toluene, with absorption and emission peaks located at 334 and 393 nm respectively, as shown in Figure S3 (Supporting Information). According to previous studies on achiral (chiral) molecules treated chiral (achiral) inorganic nanocrystals,[36,46–50] we can envisage two mechanisms that are responsible for the chirality transfer from chiral NPLs to C440 molecules via direct binding: i) the chiral configuration of C440 molecules at NPLs' surface, and ii) their electronic coupling with NPL's core. Following the chiral twisted shape of $CsPbBr_3$ NPLs, C440 molecules binding at the surface could also adopt a chiral configuration, similar to previous reports of achiral organic molecules attached at the surface of chiral metal or semiconductor nanocrystals.[36,48,49] Also, electronic coupling between surface C440 molecules and NPL's core is expected to be operative here, like in the case of chiral dyes or ligands-treated semiconductor nanocrystals where decreased coupling distance resulted in an enhanced optical activity.[45–47,50] Based on those two potential mechanisms, chirality transfer can occur from the chiral perovskite NPLs to the bound molecules, leading to UVCPL emission appearing under excitation at 320 nm, as illustrated in Figure 1C.

For realizing UVCPL emission via the TET process, another molecule – 9-phenanthrene carboxylic acid (Figure 1B, which will be abbreviated as 9-PCA later on) has been used as a triplet transmitter to fabricate nanocrystal-molecular hybrids because of its suitable triplet energy $E_T \approx 2.64$ eV and the presence of carboxylic groups for binding at the NPLs' surface.[51] Also, triplet annihilators such as 2,5-diphenyloxazole (PPO) with a lower triplet energy of $E_T \approx 2.3$ eV are necessary for facilitating the TET-2 process and finally realizing UVCPL emission via the TTA-UC process.[38,51–53] As illustrated in Figure 1D, when $CsPbBr_3$ NPLs

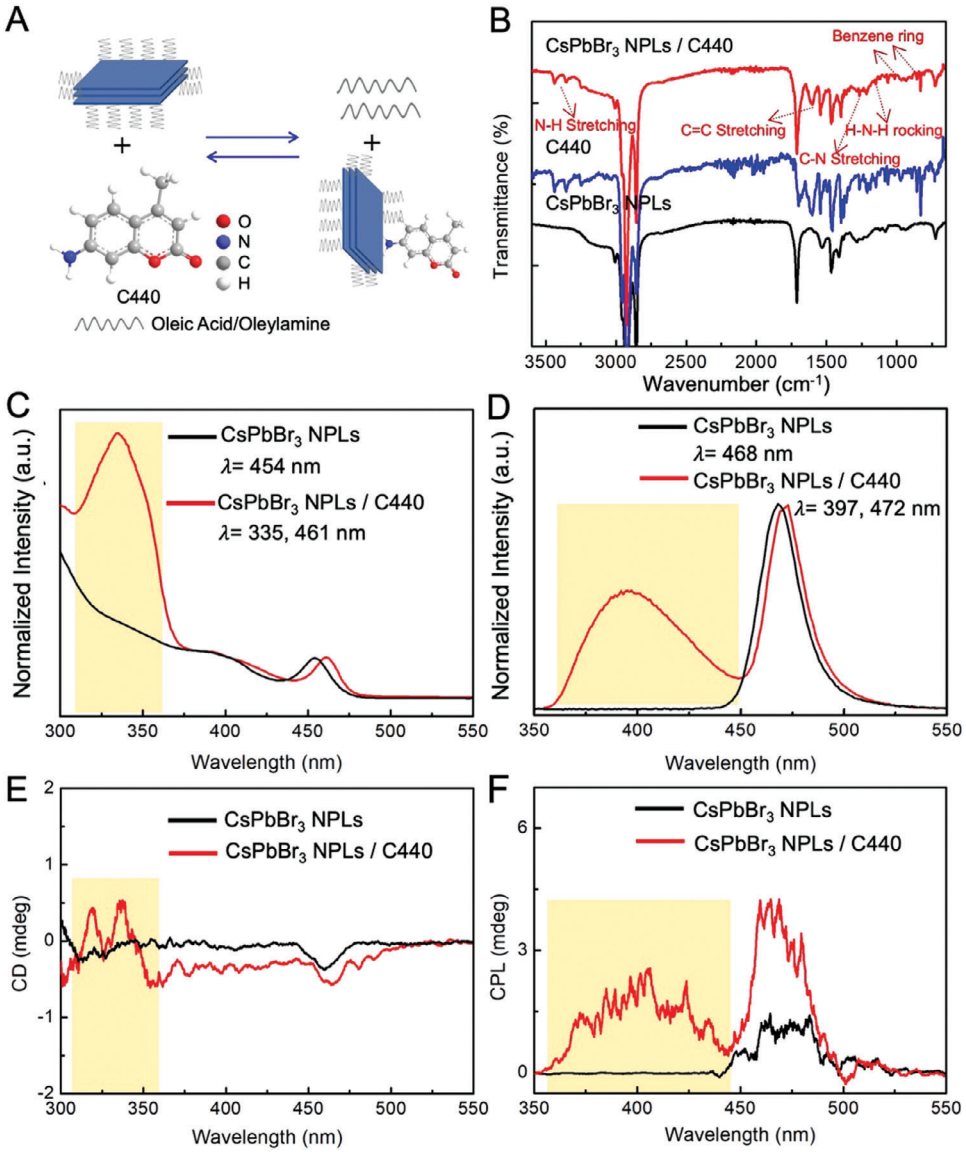

Figure 2. UVCPL was realized via a direct binding approach in hybrids of $CsPbBr_3$ NPLs and C440. A) Illustration of the post-treatment process used for fabrication of $CsPbBr_3$ NPLs/C440 hybrids. B) FTIR spectra of $CsPbBr_3$ NPLs/C440 hybrids (red), pristine C440 (blue), and pristine $CsPbBr_3$ NPLs (black). Absorption (C) and PL (D), as well as the corresponding CD (E) and CPL spectra (F) recorded from pristine $CsPbBr_3$ NPLs (black) and from $CsPbBr_3$ NPLs/C440 hybrids (red).

are excited selectively by a 450 nm laser, the triplet energy can be transferred from chiral $CsPbBr_3$ NPLs to surface-binding 9-PCA (TET-1 process) and then to unbound PPO present in solution (TET-2 process), which would then emit UVCPL via a TTA-UC process when two PPO triplets encounter. In this case, achiral annihilators of PPO can only harvest energy from chiral NPLs via the TET process, resulting in enhanced UVCPL emission. In the following, we will employ a series of optical measurements to experimentally validate the occurrence of the aforementioned scenarios.

We first examined the UVCPL emission from $CsPbBr_3$ NPLs/C440 hybrids. 3 ML $CsPbBr_3$ NPLs with intrinsic chirality were synthesized through a modified anti-solvent recrystallization process,[42] and treated by an eightfold molar excess of C440 in toluene relative to $CsPbBr_3$ NPLs (**Figure 2A**, see Experimental Section for details). Similar to what has been reported previously, where organic ligands with amine groups could replace some of the native ligands at the surface of $CsPbBr_3$ nanocrystals,[54–56] C440 binds at the surface of $CsPbBr_3$ NPLs, as confirmed by Fourier Transform infrared (FTIR) spectroscopy and optical data. FTIR spectra in Figure 2B show that characteristic vibration modes of the amine group and the benzene ring are present in the $CsPbBr_3$ NPLs/C440 hybrids. In detail, after being treated with C440, two characteristic peaks appear at 3436 and 3355 cm^{-1}, which are assigned to the N—H asymmetric and symmetric stretching modes of the amine group in C440.[57] Two more peaks of the amine group ($-NH_2$) are detected at 1266 and 1147 cm^{-1}, corresponding to the C—N stretching and

H—N—H rocking vibration modes, respectively.[57] Furthermore, when compared with pristine $CsPbBr_3$ NPLs, a peak emerges at 1602 cm^{-1} which is a typical feature of the C═C stretching mode in C440 molecules.[57] Also, the benzene ring of C440 in hybrids gives two more characteristic peaks at 856 and 1014 cm^{-1}, corresponding to the ring breathing and CCC trigonal bending modes, respectively.[57]

When comparing the optical spectra, after treatment with C440 molecules, a significant enhancement in the absorbance at ≈335 nm is observed in hybrids (Figure 2C) as compared to pristine NPLs, which is because of the absorption of C440 molecules (Figure S3, Supporting Information); in contrast, pristine $CsPbBr_3$ NPLs only show a sharp peak at 454 nm. Also in the PL spectra of the hybrids shown in Figure 2D, the emission band from C440 molecules binding at the surface of NPLs appears at 397 nm. The PL emission of binding C440 molecules experiences a red-shift to a longer wavelength as compared to free C440 molecules in toluene (Figure S3, Supporting Information), which may be due to interactions between neighboring ligands at the NPLs' surface.[36] Absorption and emission maxima of $CsPbBr_3$ NPLs also slightly shift to longer wavelength after being treated with C440 molecules.

Circular dichroism (CD) and CPL measurements were then conducted to analyze the chiroptical properties of hybrids and to reveal the chirality transfer from $CsPbBr_3$ NPLs to C440 molecules. As reported previously,[42] pristine $CsPbBr_3$ NPLs show a negative CD band corresponding to the first exciton absorption due to the chiral twisted shape induced by naturally formed screw dislocations; after treatment, achiral C440 binding at NPLs' surface would follow the chiral twisted shape of $CsPbBr_3$ NPLs and adopt a chiral configuration, thus leading to the emergence of new CD peaks assigned to C440 absorption, as evidenced from Figure 2E. In addition, as mentioned above, electronic coupling between NPL's core and surface C440 molecules may also assist the chirality transfer from NPLs to C440 molecules, like in previous reports on chiral dyes or ligands-treated semiconductor nanocrystals.[45–47,50] As shown in Figure 2F, UVCPL emission from C440 molecules binding at the surface is recorded with the dissymmetry factor g_{lum} of 6.8×10^{-4}. Similar to the trends observed for the absorption and PL emission spectra, both CD and CPL spectra of $CsPbBr_3$ NPLs experience a similar red shift after being treated with C440. Importantly, the optical activity of $CsPbBr_3$ NPLs is enhanced 2 times after being treated with C440 molecules, and asymmetric g-factors of CD and CPL emission increased from 2.5×10^{-5} and 2.4×10^{-4} to 4.8×10^{-5} and 5.5×10^{-4}, respectively (Figure S4, Supporting Information), which again confirms that the C440 molecules bind at NPLs' surface with a chiral configuration, leading to enhanced CD and CPL signals of $CsPbBr_3$ NPLs. Additionally, no noticeable energy transfer from C440 to $CsPbBr_3$ NPLs is observed, as confirmed by time-resolved photoluminescence (TRPL) data in Figure S5 (Supporting Information). In summary, we have realized chirality transfer from chiral NPLs to C440 molecules by direct binding and thus observe efficient UVCPL emission.

For realizing UVCPL via the TET process, $CsPbBr_3$ NPLs with intrinsic chirality and optical band gap of 2.66 eV were employed as triplet sensitizers; **Figure 3A(i)** shows their absorption and PL emission spectra. 9-PCA and PPO with UV absorption and emission spectra shown in Figure 3A(ii,iii) were selected as triplet transmitters and annihilators, respectively, due to their suitable triplet energy level with respect to $CsPbBr_3$ NPLs, which should favor TET and TTA-UC process for realizing UVCPL. When NPLs are excited at 400 nm selectively, PPO could harvest triplets from chiral NPLs via surface-bound 9-PCA, and then emit UVCPL when two PPO triplets encounter, as illustrated in Figure 1D. We have performed the surface treatment of $CsPbBr_3$ NPLs with 9-PCA (the samples made will be denoted as $CsPbBr_3$ NPLs/9-PCA later on) in a similar way as in the case of C440 treatment (see Experimental Section for details). As reported previously,[28,38,51] 9-PCA has low solubility in toluene and tends to replace some parts of native ligands at the NPLs' surface. Indeed, besides the absorption features of $CsPbBr_3$ NPLs, a new peak appears around 300 nm in the absorption (Figure 3B) and CD spectra (Figure S6, Supporting Information) of $CsPbBr_3$ NPLs/9-PCA hybrids, indicating the attachment of some 9-PCA molecules. The binding of 9-PCA has also been confirmed by FTIR spectra in Figure S7 (Supporting Information), where characteristic vibration modes of the carboxylic acid and the phenanthrene ring are present in the $CsPbBr_3$ NPLs/9-PCA hybrids. For example, aromatic C—H stretching is observed at 3043 cm^{-1}, and the skeleton vibration of the phenanthrene ring appears at 1528, 1498, and 1443 cm^{-1} (between 1400–1620 cm^{-1}).[58] Also, two peaks corresponding to COO^- asymmetric and symmetric stretching vibrations are recorded at 1684 and 1414 cm^{-1} respectively, and the peak at 1291 cm^{-1} relates to C—O stretching vibrations of carboxylate.[58,59] Moreover, as compared with pristine NPLs, significant PL quenching is detected in the PL spectra of $CsPbBr_3$ NPLs/9-PCA hybrids (Figure 3B); while after adding PPO (denoted as $CsPbBr_3$ NPLs/9-PCA/PPO later on), a further quenching happens.

TET from perovskite NPLs to 9-PCA (TET-1 process) and then to PPO (TET-2 process) are both critical for realizing UVCPL (Figure 1D) and thus TRPL measurements were performed to characterize these processes. The evidence that the TET-1 process occurs is obtained from the comparison of nanosecond PL decays of pristine NPLs and $CsPbBr_3$ NPLs/9-PCA hybrids shown in Figure 3C, as well as $CsPbBr_3$ NPLs/9-PCA/PPO hybrids shown in Figure S8 (Supporting Information). These TRPL decays can be fitted by two exponential functions (see detailed parameters in Table S1, Supporting Information). Compared with pristine NPLs (the average PL lifetime of 3.6 ± 0.16 ns), the average PL lifetime of $CsPbBr_3$ NPLs/9-PCA (0.84 ± 0.02 ns) is shortened considerably due to the occurrence of TET-1 process from NPLs to surface-bound 9-PCA molecules; these values agree well with previous studies on related systems.[38,39,51] From TRPL decays, the rate of $k_{TET\text{-}1}$ and its efficiency $\Phi_{TET\text{-}1}$ can be calculated as approximately 0.91 ns^{-1} and 76.7%, according to[38]:

$$k_{TET-1} = \frac{1}{\tau_{NPL\ /\ 9-PCA}} - \frac{1}{\tau_{NPL}} \quad (1)$$

$$\Phi_{TET-1} = 1 - \frac{\tau_{NPL\ /\ 9-PCA}}{\tau_{NPL}} \quad (2)$$

where $\tau_{NPL/9\text{-}PCA}$ and τ_{NPL} denote the average PL lifetimes of $CsPbBr_3$ NPLs/9-PCA hybrids and pristine NPLs, respectively. The latter value of the $\Phi_{TET\text{-}1}$ can also be obtained taking into account the calculated PL quenching efficiency of ≈70.2% for

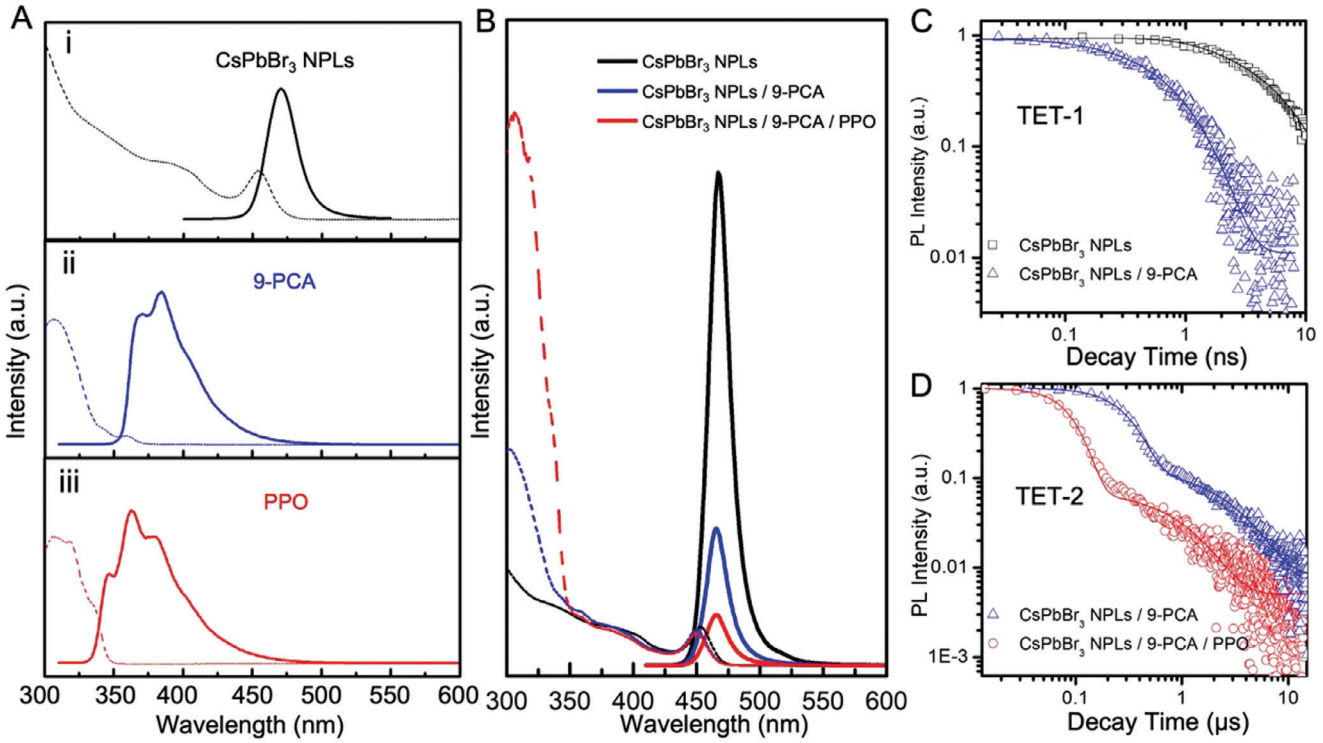

Figure 3. A) Absorption (dash) and PL (solid) spectra of $CsPbBr_3$ NPLs (i, black), 9-PCA (ii, blue), and PPO (iii, red). B) (A) Absorption (dash) and PL (solid) spectra of $CsPbBr_3$ NPLs (black), $CsPbBr_3$ NPLs/9-PCA (blue), and $CsPbBr_3$ NPLs/9-PCA/PPO (red). The NPLs' amount is the same in all three samples. C) TRPL profiles of $CsPbBr_3$ NPLs (black), and $CsPbBr_3$ NPLs/9-PCA (blue) recorded in the range of 10 ns. D) TRPL profiles of $CsPbBr_3$ NPLs/9-PCA (blue) as well as $CsPbBr_3$ NPLs/9-PCA/PPO (red) recorded in the range of 10 μs.

$CsPbBr_3$ NPLs/9-PCA shown in Figure 3B. The occurrence of the TET-2 process is evidenced by the comparison of microsecond PL decays of $CsPbBr_3$ NPLs/9-PCA and $CsPbBr_3$ NPLs/9-PCA/PPO hybrids shown in Figure 3D. The back transfer of triplets from the sensitized PCA arising from the surface-binding of 9-PCA to the NPLs means that $CsPbBr_3$ NPLs are consequently expected to show a slower PL decay component after being treated with 9-PCA.[38,60–62] It is expected that the prolonged PL lifetime of $CsPbBr_3$ NPLs/9-PCA hybrids would be largely decreased when annihilator PPO is present and the TET-2 process occurs. TRPL measurements agree well with these expectations. The PL decays shown in Figure 3D can be fitted by two-exponential functions, where the short and long lifetimes correspond to exciton radiative recombination and thermally activated emission respectively,[62] verifying the TET transfer from surface-binding 9-PCA to perovskite NPLs. In addition, the long lifetime shortens from 2.65 ± 0.06 to 0.99 ± 0.03 μs after the addition of PPO, suggesting that the TET-2 process takes place from $CsPbBr_3$ NPLs/9-PCA hybrids to PPO. Similar to the TET-1 process, the TET-2 rate and its efficiency are calculated as ≈0.63 μs^{-1} and 62.6%, respectively, from the TRPL decays. These results show that the triplet energy transfer from NPLs to surface-binding 9-PCA (TET-1 process) and then to PPO (TET-2 process) indeed occurs, and suggests the possibility of realizing UVCPL via the TET process.

TA measurements were then carried out to analyze the carrier dynamics of pristine $CsPbBr_3$ NPLs and the $CsPbBr_3$ NPLs/9-PCA hybrids, and thus uncover TET from NPLs to 9-PCA. Following the pumping by a 400 nm femtosecond (fs) laser which excites $CsPbBr_3$ NPLs selectively, TA spectra at selected delay times were recorded from pristine NPLs and their corresponding hybrids shown in **Figure** 4A,B, respectively. To exclude potential influences of multi excitonic effects, the average number of photogenerated excitons per NPL (<N>) was kept much ˂1 during all TA measurements. Both samples share similar TA spectra which are dominated by an exciton ground state photobleaching signal (PB) centered at ≈454 nm, featuring a sharp negative absorption band. The PB signal is contributed by the state-filling effects of photogenerated excitons (or electron-hole pairs) in $CsPbBr_3$ NPLs.[39,63] However, as compared with pristine NPLs, a much faster decay of the PB signal is observed from $CsPbBr_3$ NPLs/9-PCA hybrids (Figure 4C), suggesting TET from photoexcited NPLs to surface-bound 9-PCA. The TA spectra obtained at a higher pump density in Figure S9 (Supporting Information) also show similar results.

The robustness of this process is further supported by a comparison between the PB decay and the corresponding TRPL kinetics probed at the PL emission peak, as shown in Figure 4D, which are in good agreement with each other. Only slight decay could be observed at an earlier time, while the major decay occurs on a ns-timescale. A slight difference in PB and TRPL decays at a very early time is usually attributed to electron/exciton trapping by the trap states.[64] These TA curves are then fitted by a two-exponential function (see detailed parameters in Table S2, Supporting Information), showing similar results to TRPL measurements. For pristine $CsPbBr_3$ NPLs, fast and slow PB decay components of 1.18 ± 0.05 and 5.10 ± 0.21 ns are revealed, with the fast decay component attributed to radiative recombination

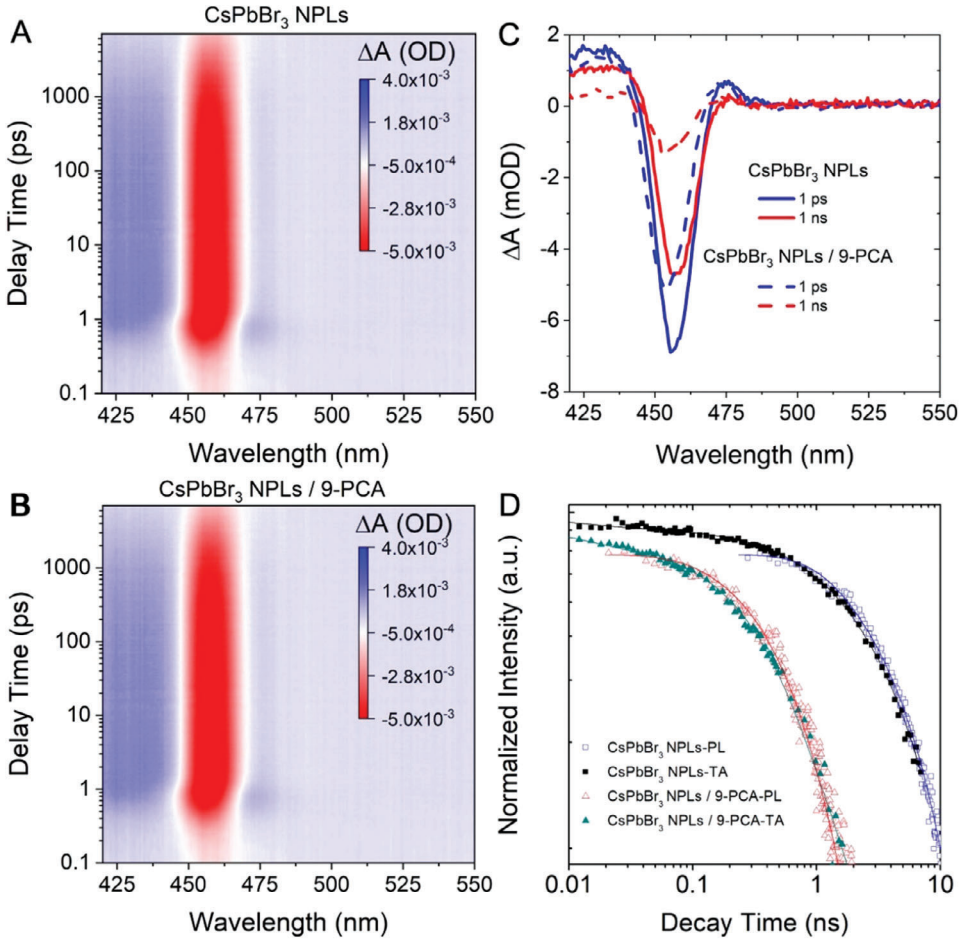

Figure 4. Characterization of the TET process via TA spectroscopy. 2D pseudo-color TA plot of pristine $CsPbBr_3$ NPLs (A) as well as $CsPbBr_3$ NPLs/9-PCA hybrids (B) at various delay times after being excited by a 400 nm pulse; the scale bar represents the optical density. C) Selected TA spectra of $CsPbBr_3$ NPLs and $CsPbBr_3$ NPLs/9-PCA hybrids at delay times of 1 ps (blue) and 1 ns (red), respectively. D) PL and PB kinetics of $CsPbBr_3$ NPLs (blue hollow and black solid squares, respectively) as well as $CsPbBr_3$ NPLs/9-PCA hybrids (red hollow and green solid triangles, respectively). Solid lines are fitting curves for the experimental data.

of the excitons, and slow decay component to recombination of trap states or dark exciton.[65–67] For $CsPbBr_3$ NPLs/9-PCA hybrids, fast and slow PB decay components are 0.49 ± 0.01 and 2.55 ± 0.15 ns, respectively. Based on the analysis of the PB decay, the average lifetime shortens from 4.01 ± 0.17 to 1.06 ± 0.05 ns for NPLs being treated with 9-PCA, corroborating the occurrence of the TET-1 process. From TA data shown in Figure 4D, the rate of TET-1 and its efficiency are calculated as 0.694 ns^{-1} and 73.6%, presenting rather similar values as those derived from TRPL analysis. Such relatively high TET-1 efficiency can be attributed to the effective wave function overlap between NPLs and surface-binding 9-PCA enabled by the strong quantum confinement effect.[38,43]

To examine the upconversion emission from $CsPbBr_3$ NPLs/9-PCA/PPO, a 450 nm continuous-wave (CW) laser is used as a pumping source to excite NPLs selectively. As a result, UV emission with three well-resolved peaks or shoulders at 326, 353, and 390 nm is observed (**Figure 5A**). These curves show a similar fine structure as the PL emission of PPO excited at 320 nm provided in Figure 3A(iii), which suggests that this emission originates from the PPO singlets. Its intensity grows rapidly with the increase of pump density, and the plot of power-dependent integrated emission intensity provides further evidence for TTA-UC emission (Figure 5B), which first grows quadratically and then turns to be linear with increasing pump density, a typical feature of the TTA-UC emission in related systems.[37,38,53] As such, quadratic and linear fits were applied to extract the TTA-UC threshold (≈0.62 W cm^{-2}) for the hybrids under study.[38,53] Yet, experimental data seems to deviate slightly from those fits, which could be due to the back TET process from 9-PCA to $CsPbBr_3$ NPLs.[38,51,53] When the excitation power is low (the quadratic regime), the TTA channel is negligible and the emission is dominated by spontaneous decay of PPO triplets via either radiative or nonradiative recombination, whereas in the high excitation power regime (the linear regime), TTA process turns to be the main channel for triplet deactivation, leading to saturated upconversion quantum yield.[38,53] Herein, its value is determined to be 0.8% by comparison with Riboflavin in ethanol as a standard, while assuming the theoretical maximum yield of 100% (see details in Experimental Section), which is rather low mainly due

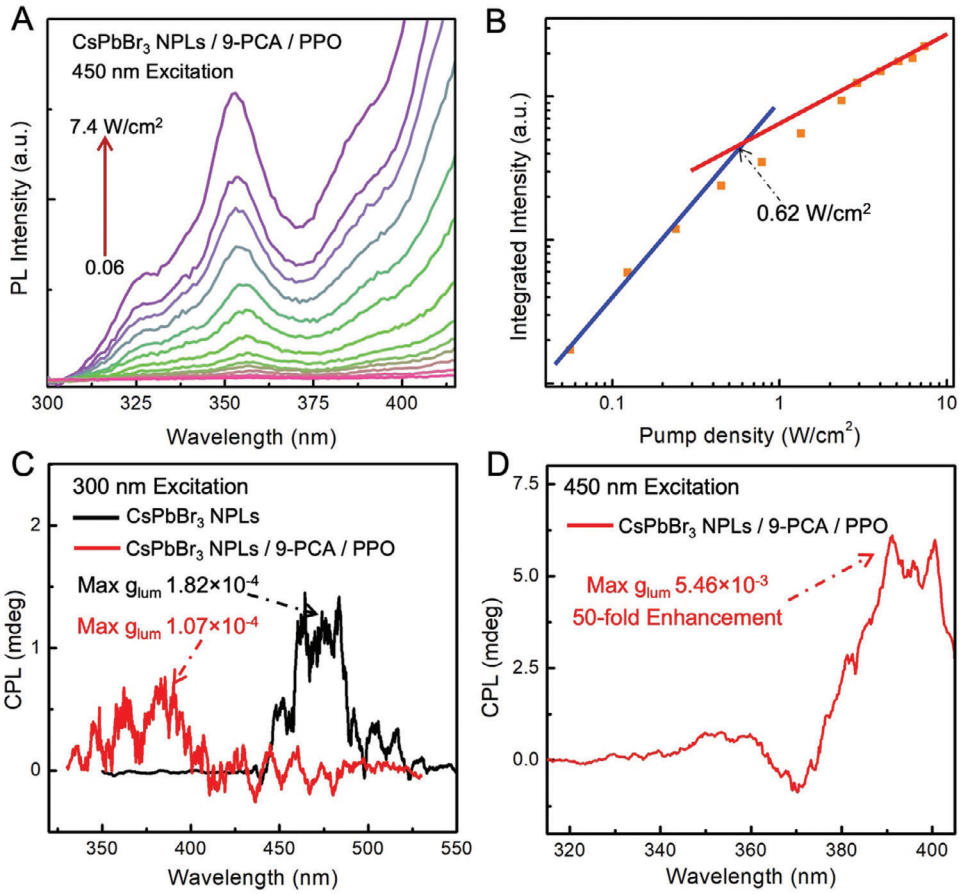

Figure 5. UVCPL is realized via the TET process. A) TTA-UC emission spectra of $CsPbBr_3$ NPLs/9-PCA/PPO hybrids were recorded at various pump densities ranging from 0.06 to 7.4 W cm^{-2}, as indicated on the frame. B) Integrated TTA-UC emission intensities as a function of pump density (orange squares for experimental results, blue and red lines for quadratic and linear fits, respectively). The crossing point indicates the TTA-UC threshold value. C) CPL spectra of $CsPbBr_3$ NPLs (black) and $CsPbBr_3$ NPLs/9-PCA/PPO hybrids (red), excited at 320 and 300 nm respectively. D) UVCPL spectra recorded from $CsPbBr_3$ NPLs/9-PCA/PPO hybrids, excited by a 450 nm CW laser.

to the low photoluminescence quantum yield of $CsPbBr_3$ NPLs induced by insufficient surface ligands coverage.[42] An apparent anti-Stokes shift is determined as 0.75 eV from the energy difference between the laser wavelength (450 nm) and the vibronic peak of PPO emission (353 nm), which is comparable to previously reported values and limited by the energy loss in the TET-2 process.[39,53]

In the following experiment, UVCPL from the $CsPbBr_3$ NPLs/9-PCA/PPO was characterized under the excitations at 300 and 450 nm, respectively. Under the excitation of 300 nm, UVCPL is observed from the hybrids and shown in Figure 5C, exhibiting a similar low luminescence dissymmetry factor g_{lum} ($\approx 1.07 \times 10^{-4}$) as compared with the pristine $CsPbBr_3$ NPLs (g_{lum} $\approx 1.82 \times 10^{-4}$). Yet, when excited selectively at 450 nm (which is above the TTA-UC threshold), UVCPL with a much higher intensity and g_{lum} of $\approx 5.46 \times 10^{-3}$ is observed (Figure 5D), resulting in an almost 50-fold enhancement compared to the value under excitation at 300 nm. Several factors may contribute to this substantial enhancement. Both UVCPL recorded under excitation at 300 and 450 nm are likely to originate from the TTA-UC process, as without the assistance of the TET process the achiral PPO only emits non-CPL light. The occurrence of TET in the $CsPbBr_3$ NPLs/9-PCA/PPO under the excitation of 300 nm is supported by the absence of CPL emission from $CsPbBr_3$ NPLs in Figure 5C. When excited at 300 nm, PL emissions coming from downconversion and the TTA-UC process both exist. The former process produces a large amount of non-CPL light, thus leading to UVCPL with a lower intensity and g_{lum}. However, this is not the case under the excitation at 450 nm, when PPO can only harvest triplets from chiral donors ($CsPbBr_3$ NPLs) and emit UVCPL. The second reason could be the perturbation of both electric and magnetic dipole transition moments of the excited states during the TET and TTA-UC process, leading to a weaker electric dipole transition and stronger magnetic dipole transition and thus promoting the CPL performance, as demonstrated by Han et al.[37,68,69] Also, the transmitter 9-PCA molecules binding at the NPLs' surface in a chiral configuration, similar to the scenario of achiral dye C440, are considered to play an important role in the CPL enhancement. In this case, the realization of UVCPL relies on TET from NPL to the surface-bound 9-PCA and then to PPO molecules in solution, which is consistent with previous reports on upconverted emission in achiral $CsPbBr_3$ nanocube-molecular hybrids;[38,60] this is strikingly different from upconverted CPL emission previously reported in chiral perovskite

nanocubes combined with upconversion nanoparticles where radiative energy transfer and chiral photon reabsorption used to play major role.[70,71] As shown in Figure S11 (Supporting Information), when the triplet transmitter 9-PCA is absent, upconverted UV and UVCPL emission is not observed from the mixture of chiral $CsPbBr_3$ NPLs and PPO in toluene, which excludes the possibility of reabsorption scenario.

Due to its higher g_{lum} value and without the necessity to have an excitation source with even higher photon energy, UVCPL occurring via the TET process is further exploited to trigger the stereoselective photopolymerization of diacetylene (DA) monomer into polydiacetylene. The experimental set-up for triggering stereoselective photopolymerization is shown in Figure S10A (Supporting Information) and includes a 450 nm CW laser, a 1 mm quartz cuvette containing the $CsPbBr_3$ NPLs/9-PCA/PPO hybrids, a short-pass filter, and a quartz substrate covered with a DA film. A 450 nm CW laser is used as the excitation source to excite NPLs selectively in the $CsPbBr_3$ NPLs/9-PCA/PPO hybrids for the realization of a UVCPL source. Behind the $CsPbBr_3$ NPLs/9-PCA/PPO sample, a 450 nm short-pass filter is placed to selectively transmit UVCPL light for triggering stereoselective photopolymerization of the DA film on the quartz substrate. After being exposed to UVCPL for 15 min, the DA film is analyzed using CD spectroscopy to confirm its stereoselective photopolymerization. According to previous reports,[20,21] the chemical process of the stereoselective photopolymerization of DA monomer into polydiacetylene is illustrated in Figure S10B (Supporting Information). When irradiated by high energy CPL light with a certain circular polarization, an addition reaction occurs among DA monomers, leading to the formation of stereoselective polydiacetylene with CD responses. A positive CD band is indeed observed from irradiated DA films (Figure S10C, Supporting Information), indicating the formation of polydiacetylene.[20] The corresponding asymmetric factor g_{abs} are also calculated and shown in Figure S10D (Supporting Information), with a maximum of 9.2×10^{-4}, which is higher than the g_{lum} of upconversion UVCPL due to the chiral amplification of stereoselective photopolymerization. Note that, the CD sign of irradiated DA film at 650 nm follows the sign of UVCPL occurring via the TET process, which agrees well with previous reports and again confirms the stereoselective photopolymerization into polydiacetylene triggered by such UVCPL.[21] In addition, to check the reliability of this CD signal, CD spectra were recorded from irradiated DA films upon the 90° rotation around the optical axis of the CD spectrometer or sample flipping. As shown in Figure S10E (Supporting Information), similar CD curves are observed.

3. Conclusion

In summary, UVCPL is realized via either direct binding or triplet energy transfer in hybrids of inorganic chiral perovskite NPLs and achiral organic molecules. $CsPbBr_3$ NPLs with chiral twisted shape are used as the source of chirality, and achiral C440 dyes bind at the NPLs' surface with a chiral configuration, thus becoming a UVCPL emitter. In another kind of hybrid, UVCPL is achieved in the chiral $CsPbBr_3$ NPLs treated with 9-PCA molecules, through the interaction with PPO molecules via TET followed by the TTA-UC process. Different from the case of the direct binding at their surface, UVCPL realized via the TET process showed a 50-fold enhanced dissymmetry factor g_{lum}. Thus, we have realized the upconversion UVCPL with a large g_{lum} of $\approx 5.46 \times 10^{-3}$ based on the TET process, and uncovered that chiral light harvesting occurs through the TTA-UC process. Moreover, due to its higher g_{lum} value and without the necessity of a higher photon energy excitation source, the stereoselective photopolymerization of diacetylene monomer is achieved by using such upconversion UVCPL. Our study offered important insights into the mechanism of excited state chirality transfer and paved the ways for realizing UVCPL, which could be extended to various material systems and broad spectral regions.

Supporting Information

Supporting Information is available from the Wiley Online Library or from the author.

Acknowledgements

B.T. and Q.W. contributed equally to this work. This work was supported by the Research Grant Council of Hong Kong SAR (CityU 11317322, PolyU 25301522, and PolyU 15301323), National Natural Science Foundation of China (22373081), Hong Kong Innovation and Technology Fund (ITS/064/22), and by the Centre for Functional Photonics (CFP) of City University of Hong Kong. The authors acknowledge Alan Leung from the Hong Kong Polytechnic University for his assistance in measuring CD and CPL spectra. This submission is dedicated to Alexander Eychmüller in honor of his retirement from the Technical University of Dresden in 2024.

Conflict of Interest

The authors declare no conflict of interest.

Data Availability Statement

The data that support the findings of this study are available in the supplementary material of this article.

Keywords

chirality transfer, metal halide perovskite nanoplatelets, nanocrystal-molecular hybrids, triplet energy transfer, UV circularly polarized luminescence

Received: December 28, 2023
Published online: January 10, 2024

[1] R. Naaman, Y. Paltiel, D. H. Waldeck, *Nat. Rev. Chem.* **2019**, *3*, 250.
[2] G. Long, R. Sabatini, M. I. Saidaminov, G. Lakhwani, A. Rasmita, X. Liu, E. H. Sargent, W. Gao, *Nat. Rev. Mater.* **2020**, *5*, 423.
[3] S. Lin, Y. Tang, W. Kang, H. K. Bisoyi, J. Guo, Q. Li, *Nat. Commun.* **2023**, *14*, 3005.
[4] H. K. Bisoyi, Q. Li, *Acc. Chem. Res.* **2014**, *47*, 3184.
[5] C. Hao, G. Wang, C. Chen, J. Xu, C. Xu, H. Kuang, L. Xu, *Nano-Micro Lett.* **2023**, *15*, 39.
[6] Y. Deng, M. Wang, Y. Zhuang, S. Liu, W. Huang, Q. Zhao, *Light: Sci. Appl.* **2021**, *10*, 76.

[7] C. Ye, J. Jiang, S. Zou, W. Mi, Y. Xiao, *J. Am. Chem. Soc.* **2022**, *144*, 9707.
[8] D. Han, C. Li, C. Jiang, X. Jin, X. Wang, R. Chen, J. Cheng, P. Duan, *Aggregate* **2022**, *3*,e148.
[9] Y. Sang, J. Han, T. Zhao, P. Duan, M. Liu, *Adv. Mater.* **2020**, *32*, 1900110.
[10] J. Ma, H. Wang, D. Li, *Adv. Mater.* **2021**, *33*, 2008785.
[11] S. Jiang, N. A. Kotov, *Adv. Mater.* **2022**, *35*, 2108431.
[12] T. Duan, Y. Zhou, *Adv. Energy Mater.* **2022**, *13*, 2200792.
[13] J. Hao, Y. Li, J. Miao, R. Liu, J. Li, H. Liu, Q. Wang, H. Liu, M.-H. Delville, T. He, K. Wang, X. Zhu, J. Cheng, *ACS Nano* **2020**, *14*, 10346.
[14] Y.-H. Kim, Y. Zhai, E. A. Gaulding, S. N. Habisreutinger, T. Moot, B. A. Rosales, H. Lu, A. Hazarika, R. Brunecky, L. M. Wheeler, J. J. Berry, M. C. Beard, J. M. Luther, *ACS Nano* **2020**, *14*, 8816.
[15] Y. Cui, J. Jiang, W. Mi, Y. Xiao, *Cell Rep. Phys. Sci.* **2023**, *4*, 101299.
[16] X. Yang, J. Lv, J. Zhang, T. Shen, T. Xing, F. Qi, S. Ma, X. Gao, W. Zhang, Z. Tang, *Angew. Chem., Int. Ed.* **2022**, *61*, 202201674.
[17] P. Liu, Y. Battie, T. Kimura, Y. Okazaki, P. Pranee, H. Wang, E. Pouget, S. Nlate, T. Sagawa, R. Oda, *Nano Lett.* **2023**, *23*, 3174.
[18] Y. Ru, B. Zhang, X. Yong, L. Sui, J. Yu, H. Song, S. Lu, *Adv. Mater.* **2023**, *35*, 2207265.
[19] A. Hubley, A. Bensalah-Ledoux, B. Baguenard, S. Guy, B. Abécassis, B. Mahler, *Adv. Optical Mater.* **2022**, *10*, 2200394.
[20] X. Jin, Y. Sang, Y. Shi, Y. Li, X. Zhu, P. Duan, M. Liu, *ACS Nano* **2019**, *13*, 2804.
[21] D. Han, X. Yang, J. Han, J. Zhou, T. Jiao, P. Duan, *Nat. Commun.* **2020**, *11*, 5659.
[22] L. Xu, H. Liu, X. Peng, P. Shen, B. Z. Tang, Z. Zhao, *Angew. Chem., Int. Ed.* **2023**, *62*, 202300492.
[23] D. T. Yonemoto, C. M. Papa, C. Mongin, F. N. Castellano, *J. Am. Chem. Soc.* **2020**, *142*, 10883.
[24] Z. Xu, Z. Huang, T. Jin, T. Lian, M. L. Tang, *Acc. Chem. Res.* **2021**, *54*, 70.
[25] J. T. Dubose, P. V. Kamat, *Chem. Rev.* **2022**, *122*, 12475.
[26] R. Weiss, Z. A. Vanorman, C. M. Sullivan, L. Nienhaus, *ACS Mater. Au* **2022**, *2*, 641.
[27] Y. Han, S. He, K. Wu, *ACS Energy Lett.* **2021**, *6*, 3151.
[28] L. Hou, A. Olesund, S. Thurakkal, X. Zhang, B. Albinsson, *Adv. Funct. Mater.* **2021**, *31*, 2106198.
[29] T. Jin, S. He, Y. Zhu, E. Egap, T. Lian, *Nano Lett.* **2022**, *22*, 3897.
[30] Z. Huang, X. Li, M. Mahboub, K. M. Hanson, V. M. Nichols, H. Le, M. L. Tang, C. J. Bardeen, *Nano Lett.* **2015**, *15*, 5552.
[31] M. Wu, T.-A. Lin, J. O. Tiepelt, V. Bulovic, M. A. Baldo, *Nano Lett.* **2021**, *21*, 1011.
[32] S. Wieghold, Z. A. Vanorman, L. Nienhaus, *Adv. Optical Mater.* **2021**, *9*, 2001470.
[33] C. Ren, W. Sun, T. Zhao, C. Li, C. Jiang, P. Duan, *Angew. Chem., Int. Ed.* **2023**, *135*, 202315.
[34] W. Liang, C. Nie, J. Du, Y. Han, G. Zhao, F. Yang, G. Liang, K. Wu, *Nat. Photonics* **2023**, *17*, 346.
[35] X. Yang, X. Jin, A. Zheng, P. Duan, *ACS Nano* **2023**, *17*, 2661.
[36] J. Kuno, N. Ledos, P.-A. Bouit, T. Kawai, M. Hissler, T. Nakashima, *Chem. Mater.* **2022**, *34*, 9111.
[37] J. Han, P. Duan, X. Li, M. Liu, *J. Am. Chem. Soc.* **2017**, *139*, 9783.
[38] S. He, Y. Han, J. Guo, K. Wu, *J. Phys. Chem. Lett.* **2022**, *13*, 1713.
[39] K. Xu, R. Li, D. Chen, J. Hu, S. Liang, H. Zhu, *Laser Photonics Rev.* **2023**, *17*, 2200572.
[40] D. M. Kroupa, D. H. Arias, J. L. Blackburn, G. M. Carroll, D. B. Granger, J. E. Anthony, M. C. Beard, J. C. Johnson, *Nano Lett.* **2018**, *18*, 865.
[41] F. J. Hofmann, M. I. Bodnarchuk, D. N. Dirin, J. Vogelsang, M. V. Kovalenko, J. M. Lupton, *Nano Lett.* **2019**, *19*, 8896.
[42] B. Tang, S. Wang, H. Liu, N. Mou, A. S. Portniagin, P. Chen, Y. Wu, X. Gao, D. Lei, A. L. Rogach, *Adv. Optical Mater.* **2023**, 2301524.
[43] X. Luo, R. Lai, Y. Li, Y. Han, G. Liang, X. Liu, T. Ding, J. Wang, K. Wu, *J. Am. Chem. Soc.* **2019**, *141*, 4186.
[44] K. Wang, R. P. Cline, J. Schwan, J. M. Strain, S. T. Roberts, L. Mangolini, J. D. Eaves, M. L. Tang, *Nat. Chem.* **2023**, *15*, 1172.
[45] X. Gao, X. Zhang, L. Zhao, P. Huang, B. Han, J. Lv, X. Qiu, S.-H. Wei, Z. Tang, *Nano Lett.* **2018**, *18*, 6665.
[46] F. Purcell-Milton, A. K. Visheratina, V. A. Kuznetsova, A. Ryan, A. O. Orlova, Y. K. Gun'ko, *ACS Nano* **2017**, *11*, 9207.
[47] V. Kuznetsova, Y. Gromova, M. Martinez-Carmona, F. Purcell-Milton, E. Ushakova, S. Cherevkov, V. Maslov, Y. K. Gun'ko, *Nanophotonics* **2020**, *10*, 797.
[48] X. Wei, J. Liu, G.-J. Xia, J. Deng, P. Sun, J. J. Chruma, W. Wu, C. Yang, Y.-G. Wang, Z. Huang, *Nat. Chem.* **2020**, *12*, 551.
[49] I. Dolamic, B. Varnholt, T. Bürgi, *Nat. Commun.* **2015**, *6*, 7117.
[50] A. K. Visheratina, A. O. Orlova, F. Purcell-Milton, V. A. Kuznetsova, A. A. Visheratin, E. V. Kundelev, V. G. Maslov, A. V. Baranov, A. V. Fedorov, Y. K. Gun'ko, *J. Mater. Chem. C.* **2018**, *6*, 1759.
[51] S. He, Y. Han, J. Guo, K. Wu, *J. Phys. Chem. Lett.* **2021**, *12*, 8598.
[52] T. N. Singh-Rachford, F. N. Castellano, *J. Phys. Chem. A* **2009**, *113*, 5912.
[53] M. Uji, T. J. B. Zähringer, C. Kerzig, N. Yanai, *Angew. Chem., Int. Ed.* **2023**, *62*, 202301506.
[54] P. Liu, W. Chen, Y. Okazaki, Y. Battie, L. Brocard, M. Decossas, E. Pouget, P. Müller-Buschbaum, B. Kauffmann, S. Pathan, T. Sagawa, R. Oda, *Nano Lett.* **2020**, *20*, 8453.
[55] Q. Cao, R. Song, C. C. S. Chan, Z. Wang, P. Y. Wong, K. S. Wong, V. Blum, H. Lu, *Adv. Optical Mater.* **2023**, *11*, 2203125.
[56] G. H. Debnath, Z. N. Georgieva, B. P. Bloom, S. Tan, D. H. Waldeck, *Nanoscale* **2021**, *13*, 15248.
[57] V. Arjunan, N. Puviarasan, S. Mohan, P. Murugesan, *Spectrochim. Acta, Part A* **2007**, *67*, 1290.
[58] M. L. Wu, M. Q. Nie, X. C. Wang, J. M. Su, W. Cao, *Spectrochim. Acta. A. Mol. Biomol. Spectrosc.* **2010**, *75*, 1047.
[59] J.-J. Max, C. Chapados, *J. Phys. Chem. A* **2004**, *108*, 3324.
[60] S. He, Y. Han, J. Guo, K. Wu, *ACS Energy Lett.* **2021**, *6*, 2786.
[61] C. Mongin, P. Moroz, M. Zamkov, F. N. Castellano, *Nat. Chem.* **2018**, *10*, 225.
[62] M. La Rosa, S. A. Denisov, G. Jonusauskas, N. D. Mcclenaghan, A. Credi, *Angew. Chem., Int. Ed.* **2018**, *57*, 3104.
[63] S. He, X. Luo, X. Liu, Y. Li, K. Wu, *J. Phys. Chem. Lett.* **2019**, *10*, 5036.
[64] Y. Wu, C. Wei, X. Li, Y. Li, S. Qiu, W. Shen, B. Cai, Z. Sun, D. Yang, Z. Deng, H. Zeng, *ACS Energy Lett.* **2018**, *3*, 2030.
[65] M. A. Becker, R. Vaxenburg, G. Nedelcu, P. C. Sercel, A. Shabaev, M. J. Mehl, J. G. Michopoulos, S. G. Lambrakos, N. Bernstein, J. L. Lyons, T. Stöferle, R. F. Mahrt, M. V. Kovalenko, D. J. Norris, G. Rainò, A. L. Efros, *Nature* **2018**, *553*, 189.
[66] M. Gramlich, M. W. Swift, C. Lampe, J. L. Lyons, M. Döblinger, A. L. Efros, P. C. Sercel, A. S. Urban, *Adv. Sci.* **2022**, *9*, 2103013.
[67] J. Li, L. Luo, H. Huang, C. Ma, Z. Ye, J. Zeng, H. He, *J. Phys. Chem. Lett.* **2017**, *8*, 1161.
[68] T. Zhao, J. Han, P. Duan, M. Liu, *Acc. Chem. Res.* **2020**, *53*, 1279.
[69] C. Corvaja, L. Franco, K. M. Salikhov, V. K. Voronkova, *Appl. Magn. Reson.* **2005**, *28*, 181.
[70] X. Yang, M. Zhou, Y. Wang, P. Duan, *Adv. Mater.* **2020**, *32*, 2000820.
[71] X. Jin, M. Zhou, J. Han, B. Li, T. Zhang, S. Jiang, P. Duan, *Nano Res.* **2022**, *15*, 1047.